MAPPING OF LUNAR SURFACE FROM SIDE-LOOKING ORBITAL RADAR IMAGES

FRANZ LEBERL*

Space Sciences Division, Jet Propulsion Laboratory, Pasadena, Calif., U.S.A.

(Received 6 January; revised 26 February, 1976)

Abstract. Side-looking spacecraft radar imagery has thus far been produced only from an orbit around the Moon. This was a part of the Apollo Lunar Sounder Experiment (ALSE) of the Apollo 17 mission in December, 1972. This paper reports results of a radargrammetric evaluation of overlapping Apollo 17 synthetic aperture radar images (wavelength 2 m). The potential to map from single images and to reconstruct 3D stereoscopic models is studied. The relative height accuracy achieved is about ± 100 m and is thus competitive with that obtained with the vidicon camera that is presently used for planetary exploration.

1. Introduction

Topographic surface relief can be measured with an accuracy of ± 100 to ± 300 m using a pair of overlapping side-looking orbital radar images of the Moon. Planimetric accuracy is somewhat lower, resulting in root mean square errors of ± 250 m to more than 1 km. These results are obtained in a radargrammetric evaluation of the mapping potential of existing orbital radar images.

Civilian orbital imaging radar was used for the first, and so far the only, time on the Apollo 17 mission to the Moon. The primary aim of the Apollo Lunar Sounder Experiment (ALSE) aboard the command module was to make radar measurements at wavelengths of 60 m, 20 m (HF) and 2 m (VHF). However, the experiment was designed in such a way that surface profiles as well as side-looking images were produced (Phillips *et al.*, 1973) during two complete lunar orbits.

The 2-m (VHF) radar returns were the most useful for mapping the lunar surface, since they recorded images from features not lying along the spacecraft track. However, even at the 2-m wavelength the lunar surface appears to be rather smooth, so that most returns are specular. The images, therefore, show less detail than with a radar of shorter wavelength.

Segments of overlapping ALSE-VHF imagery produced during orbits 25 and 26 of the Apollo 17 command module over crater Maraldi (19°N, 35.5°E) were the basis for the study of the radargrammetric potential of this data (Figure 1(a) and (b)). Figure 2 shows a portion of an Apollo 17 metric photograph of the same area. The present paper describes methods for the radargrammetric mapping of surface features and analyzes their results. Conclusions from this analysis are of value for radar mapping of previously unexplored areas of the lunar far side and for the exploration of the planet Venus with an imaging radar (Rose and Friedman, 1974).

* NAS–NRC Resident Research Associate.

The Moon **15** (1976) 329–342.

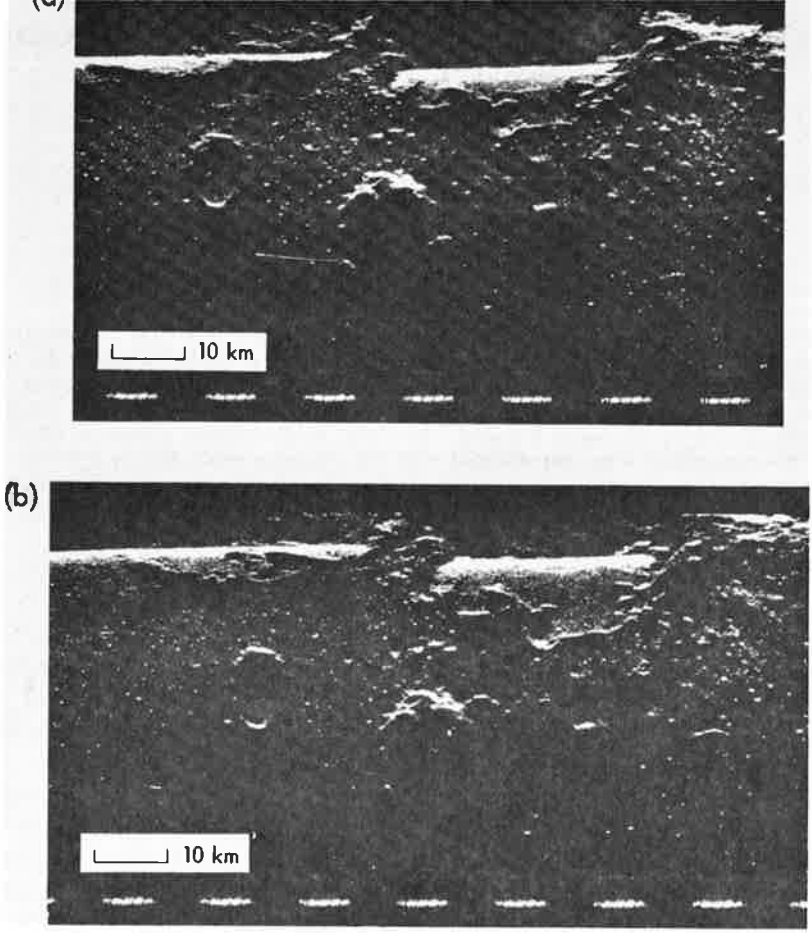

Fig. 1. ALSE-VHF side-looking orbital radar images of crater and Mons Maraldi on the Mo produced aboard the Apollo 17 command module (a) during revolution 25 and (b) dur revolution 26.

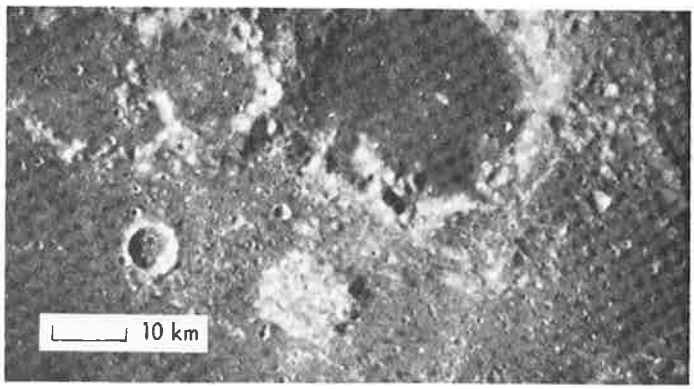

Fig. 2. Section of the Apollo 17 metric frame photograph No. 1495 of the crater and Mons Maral

2. Mathematical Model for Orbital Radargrammetry

A. INNER ORIENTATION

A rectangular x, y coordinate system can be defined in the radar images by pointing the x-axis in the direction of film transport (orbit direction) and the y-axis in range direction. Inner orientation relates these image coordinates to the physical quantities measured by the radar: namely, time t and slant range r as given by

$$t = x/c_1, \tag{1}$$

$$r = (y/c_2 + c_3)\, c_0/2, \tag{2}$$

where c_1 is the film transport velocity, c_2 the velocity of the flying spot across the screen of the radar display cathode ray tube, c_3 is a constant sweep delay, and c_0 is the speed of electromagnetic radiation. Equations (1) and (2), apply to the particular case of slant range presentation and constant film transport velocity as in ALSE-radar. Other relations might apply to other radars.

B. PROJECTION EQUATIONS

Time t (Equation 1) relates the radar image to the spacecraft trajectory. A convenient form of describing this trajectory at time t is with a position vector $\mathbf{s} = (s_1, s_2, s_3)$ and its first derivative, velocity vector $\dot{\mathbf{s}}$, in a selenocentric right-hand coordinate system rotating with the Moon (Figure 3). Each radar image point leads

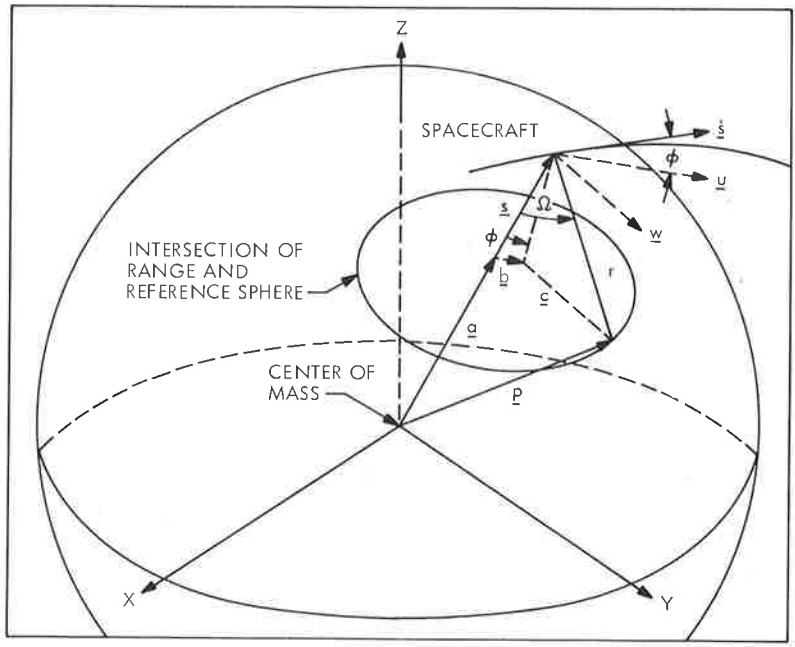

Fig. 3. Coordinate system and vectors for radargrammetry.

therefore to the following pair of equations for the unknown surface point deno by position vector $\mathbf{p}$ (Konecny, 1970)

$$|\mathbf{p} - \mathbf{s}| = r, \tag{3a}$$

$$\dot{\mathbf{s}} \cdot (\mathbf{p} - \mathbf{s}) = 0. \tag{3b}$$

Equation (3a) is the spherical locus of points at slant range r from the anter center. Equation (3b) is a plane perpendicular to velocity vector $\dot{\mathbf{s}}$ and thus represe the locus of points with zero-doppler frequency. (Vectors are denoted as underli lower case letters. Matrices are underlined upper case letters. The two vertical b ($\|$) denote the length of the vector.)

The unknown vector $\mathbf{p}$ can be expressed as an explicit function of $\mathbf{s}$, $\dot{\mathbf{s}}$ and r, i new unknown elevation angle Ω is introduced in a vector $\mathbf{q}$ defined by

$$\mathbf{q} = r\,(0, \sin\Omega, -\cos\Omega)^T,$$

$$\mathbf{p} = \mathbf{s} + \mathbf{A}\mathbf{q}.$$

The rotation matrix $\mathbf{A}$ contains the velocity vector $\dot{\mathbf{s}}$ (Leberl, 1975).

C. INTERSECTION OF THE RADAR PROJECTION RAY AND A SPHERE

Mapping from a single orbital radar image is accomplished by intersecting t radar projection rays with the lunar reference sphere of radius SR. It can m efficiently and unambiguously be done with an approach based on Figure 3. Fr this figure, it is obvious that

$$\mathbf{p} = \mathbf{a} + \mathbf{b} + \mathbf{c},$$

where (note that $|\mathbf{p}| = SR$)

$$\mathbf{a} = \mathbf{s}\,(SR^2 + |\mathbf{s}|^2 - r^2)/(2|\mathbf{s}|^2), \tag{4}$$

$$\mathbf{b} = \mathbf{u}\,(|\mathbf{s}| - |\mathbf{a}|)\tan\phi, \qquad \cos\phi = \mathbf{u} \cdot \dot{\mathbf{s}}/|\dot{\mathbf{s}}| \tag{5}$$

$$\mathbf{c} = \mathbf{w}\,(r^2 - |\mathbf{b}|^2 - (|\mathbf{s}| - |\mathbf{a}|)^2)^{1/2}; \tag{6}$$

and unit vectors $\mathbf{w}$, $\mathbf{u}$ result from

$$\mathbf{w} = (\dot{\mathbf{s}} \times \mathbf{s})/|\dot{\mathbf{s}} \times \mathbf{s}|, \tag{7}$$

$$\mathbf{u} = (\mathbf{w} \times \mathbf{s})/|\mathbf{w} \times \mathbf{s}|. \tag{8}$$

D. FORMATION OF A RADARGRAMMETRIC STEREO MODEL

A stereo model can be formed by solving two pairs of Equation (3) with t unknown vector $\mathbf{p}$. Denoting the two radar images by ($'$) and ($''$), one has thus solve $\mathbf{p} = (p_1, p_2, p_3)$ from

$$|\mathbf{p} - \mathbf{s}'| = r', \qquad |\mathbf{p} - \mathbf{s}''| = r'',$$

$$\dot{\mathbf{s}}' \cdot (\mathbf{p} - \mathbf{s}') = 0, \qquad \dot{\mathbf{s}} \cdot (\mathbf{p} - \mathbf{s}'') = 0. \tag{9}$$

Solution of these 4 equations with 3 unknowns requires a least-squares algorithm. Linearization leads to

$$\mathbf{C}\,\mathbf{v} + \mathbf{D}\,\Delta\mathbf{p} + \mathbf{w} = 0. \tag{13}$$

Vector $\mathbf{v}$ contains the corrections to observations $\mathbf{s}'$, $\mathbf{s}''$, $\dot{\mathbf{s}}'$, $\dot{\mathbf{s}}''$, r', and r''. Vector $\Delta\mathbf{p}$ contains the corrections to approximate values of vector $\mathbf{p}$. Vector $\mathbf{w}$ contains contradictions, and $\mathbf{C}$, $\mathbf{D}$ are coefficient matrices. With $\mathbf{G}$ the weight matrix of the observations, the unknown $\Delta\mathbf{p}$ and its variance-covariance matrix $\mathbf{Q}_p$ result from

$$\begin{aligned} \mathbf{Q}_p &= (\mathbf{D}^T\,(\mathbf{C}\,\mathbf{G}^{-1}\,\mathbf{C}^T)^{-1}\,\mathbf{D})^{-1}, \\ \Delta\mathbf{p} &= -\mathbf{Q}_p\,\mathbf{D}^T\,(\mathbf{C}\,\mathbf{G}^{-1}\,\mathbf{C})^{-1}\,\mathbf{w}. \end{aligned} \tag{14}$$

This approach minimizes the weighted square sum of corrections $\mathbf{v}^T\mathbf{G}^{-1}\mathbf{v}$. But an alternative approach is based on two sets of Equations (5) which result in

$$\mathbf{A}\,\mathbf{q}' + \mathbf{s}' - \mathbf{A}''\,\mathbf{q}'' - \mathbf{s}'' = 0. \tag{15}$$

These are 3 equations with the 2 unknown elevation angles Ω', Ω''. Linearization leads to

$$\mathbf{E}\,\Delta\boldsymbol{\Omega} + \mathbf{w} = \mathbf{v}, \tag{16}$$

$$\Delta\boldsymbol{\Omega} = -(\mathbf{E}^T\,\mathbf{G}\,\mathbf{E})^{-1}\,\mathbf{E}^T\,\mathbf{G}\,\mathbf{w}. \tag{17}$$

Vector $\mathbf{v}$ contains the components v_x, v_y, v_z of the minimum distance between the two projection rays. It is this distance which is minimized in approach (17).

E. SIMPLIFIED RADAR MAPPING EQUATIONS

For mapping of the relative location of features of a small area, the orbits can be approximated by straight line elements parallel to the surface. A simplified set of formulas can convert the image coordinates into a local rectangular XYZ system (Figure 4). One finds for a single image that

$$X = x(f), \tag{18a}$$

$$Y = (r^2 - H^2)^{1/2}; \tag{18b}$$

and for a stereo pair,

$$X = (x' + x'')f/2, \tag{19a}$$

$$Y = (r''^2 - r'^2 - B^2)/(2B), \tag{19b}$$

$$Z = H - ((r'^2 - Y^2)^{1/2} + (r''^2 - (Y + B)^2)^{1/2})/2; \tag{19c}$$

where H is the orbit height above the surface, B is the stereo base, and f is a scale factor.

F. USE OF GROUND CONTROL POINTS

Adjustment of radargrammetric data to given ground control points can be interpolative or parametric (Leberl, 1972; Baker *et al.*, 1975). In the interpolative case, transformation of the radar image data into object space coordinates proceeds

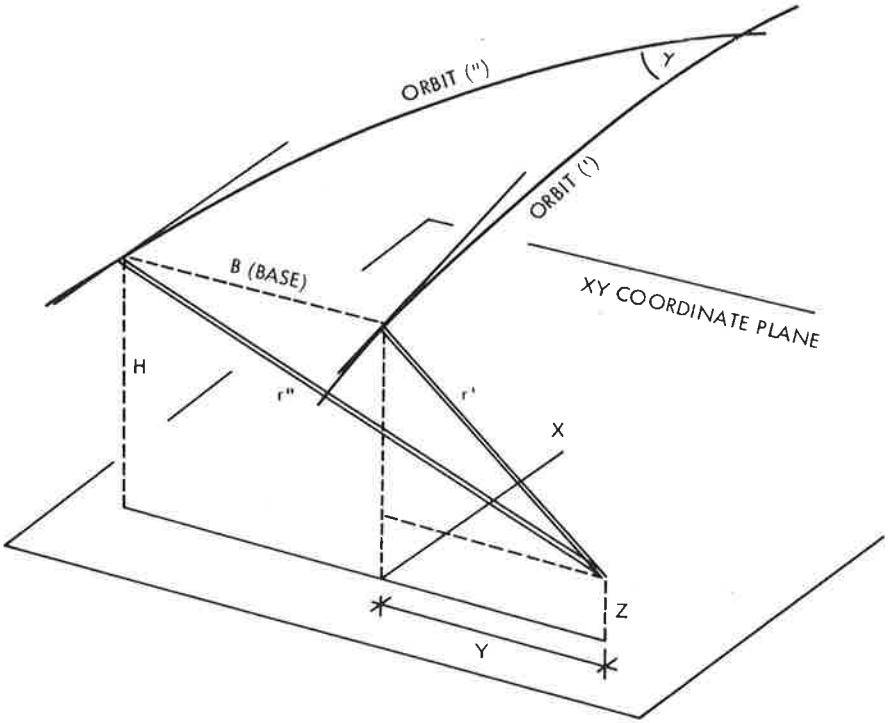

Fig. 4. Entities for simplified orbital radargrammetry.

without use of ground control points. However, the radargrammetric coordinates a ground control point will differ from the known object coordinates. This differer can be used to interpolate corrections in all radargrammetric points.

An efficient parametric use of ground control points is based on Figure 5. T observed orbit is represented by a linear spline function, thus consisting of lin pieces i that begin at the end point of $\mathbf{s}_i$ and point along velocity vector $\dot{\mathbf{s}}_i$. T orbit position at which a ground control point with position vector $\mathbf{g}$ was imag can be computed by defining the zero-doppler plane normal to the orbit a passing through the end point of $\mathbf{g}$. From Figure 5 one can see that

$$e = \dot{\mathbf{s}}_i \cdot (\mathbf{s}_i - \mathbf{g}), \qquad \mathbf{s} = \mathbf{s}_i + \dot{\mathbf{s}}_i(e/|\dot{\mathbf{s}}_i|). \tag{2}$$

Once vector $\mathbf{s}$ is computed, it leads to slant range r and time t of imaging. The however, are also independently obtained from the radar images. The discrepanc Δr, Δt can be used to calibrate the radargrammetric range and time measuremen It is proposed that this be done with the polynomials

$$\Delta r = a_0 + a_1\, x + a_2\, x^2 + a_3\, x^3 + a_4\, y + a_5\, yx + a_6\, x^2\, y + \cdots, \tag{21}$$

$$\Delta t = b_0 + b_1\, x + b_2\, x^2 + b_3\, x^3 + \cdots. \tag{21}$$

The polynomial (21a) is chosen linear in the cross-track coordinate directio Differentiation of Equation (2) shows that non-linear variation of Δr is not necessar

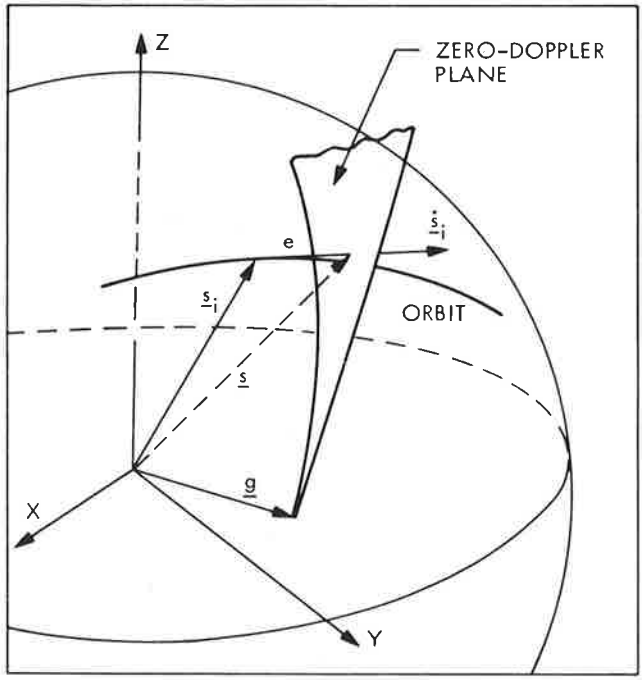

Fig. 5. Geometry of intersection of orbit and zero-doppler plane through ground control point defined by vector **g**.

expected. This conclusion has been experimentally confirmed by Gracie *et al.* (1970). In orbit direction, however, image coordinate errors are non-linear; the calibration polynomials (21) should be so, also.

3. Radargrammetric Results with ALSE-VHF Imagery

3.1. INPUT DATA

Evaluation of the mapping potential of side-looking orbital radar is based on the pair of ALSE-VHF images shown in Figure 1. The radargrammetric results are compared with photogrammetrically procured lunar coordinates. About 70 points were identified in a pair of Apollo 17 metric photographs and the ALSE image covering an area of about 100 × 40 km^2 around crater and Mons Maraldi. This area was selected because of surface relief in excess of 1000 m, good stereo viewability and availability of topographic maps.

Table I summarizes relevant information about the images and measurements. The ALSE radar system could record the returns from off-nadir angles of up to about 22° (to both sides of the track – see maximum and minimum elevation angles). The radar beam, however, was shaped such that the returns were obtained essentially from the surface to the right of the track, whereas returns from the area to the left were received only from angles of up to 5° off-vertical. But occasionally, radar echoes are received from lunar features to the left of the track at angles larger than

TABLE I

Parameters of ALSE-VHF radar and Apollo 17 metric photography

Metric photography		Radar imagery	
Principal distance	75.842 mm	Orbital altitude	116
Scale	1 : 1 500 00	Stereobase	3
Photograph Nos.	AS 1495, 1497	Max elevation angle	22
Overlap	60%	Min elevation angle	
Predicted height accuracy	±30 m	Theoretical	−22
		Practical	−5
Rms discrepancy between comparator and stereo plotter models	±30 m	Sweep delay	746.2
		Along-track scale	1 : 1000
Rms discrepancy between map and stereo model		Across-track slant range scale	1 : 210
Planimetry	±300 m		
		Wavelength	
Height	±100 m	Resolution (slant)	1
Diameter of marked points	70 μm	Resolution (ground)	30 to 15
		Diameter of marked points	70

5° off-nadir. The returns from the left and the right of the track are superimpos in the image, as seen in the upper portion of Figure 1a and 1b.

Further comment to Table I concerns the across-track slant range scale: across-track image coordinates y have to be multiplied with a constant scale fac of about 210 000 to obtain slant ranges. However, due to the steep look angles the ALSE radar, the effective across-track image scale is smaller than 1 : 210 0 It is variable across the image: for a look angle of 15° off-nadir, the effective acr track image scale number is 1/sin 15° times the slant range scale number, th approximating the along-track scale as is apparent in the radar images of Figure

The lunar surface points that were identified on the metric photograph and radar images were marked and measured on a Mann monocomparator (10× opti enlargement) and OMI-Analytical Plotter APC (14× optical enlargement). addition to the identifiable points, a digital height model of Mons Maraldi w procured from the metric and radar-stereo models. For the latter, it was found th not more than a 6× enlargement should be used for best stereovision.

The radar images display a range reference line which was chosen as ima x-coordinate axis. Available time marks allowed a somewhat inaccurate relati between an image and the spacecraft trajectory.

The metric photography was reduced in a standard photogrammetric procedu to serve as a reference for comparison with radargrammetric data.

B. PREDICTED RADARGRAMMETRIC ACCURACY

The mapping potential of ALSE-VHF imagery can be predicted theoretically statistical error propagation based on Equation (18) and (19). Figure 6 presents t result. For single-image radargrammetry (Figure 6a), the most significant err

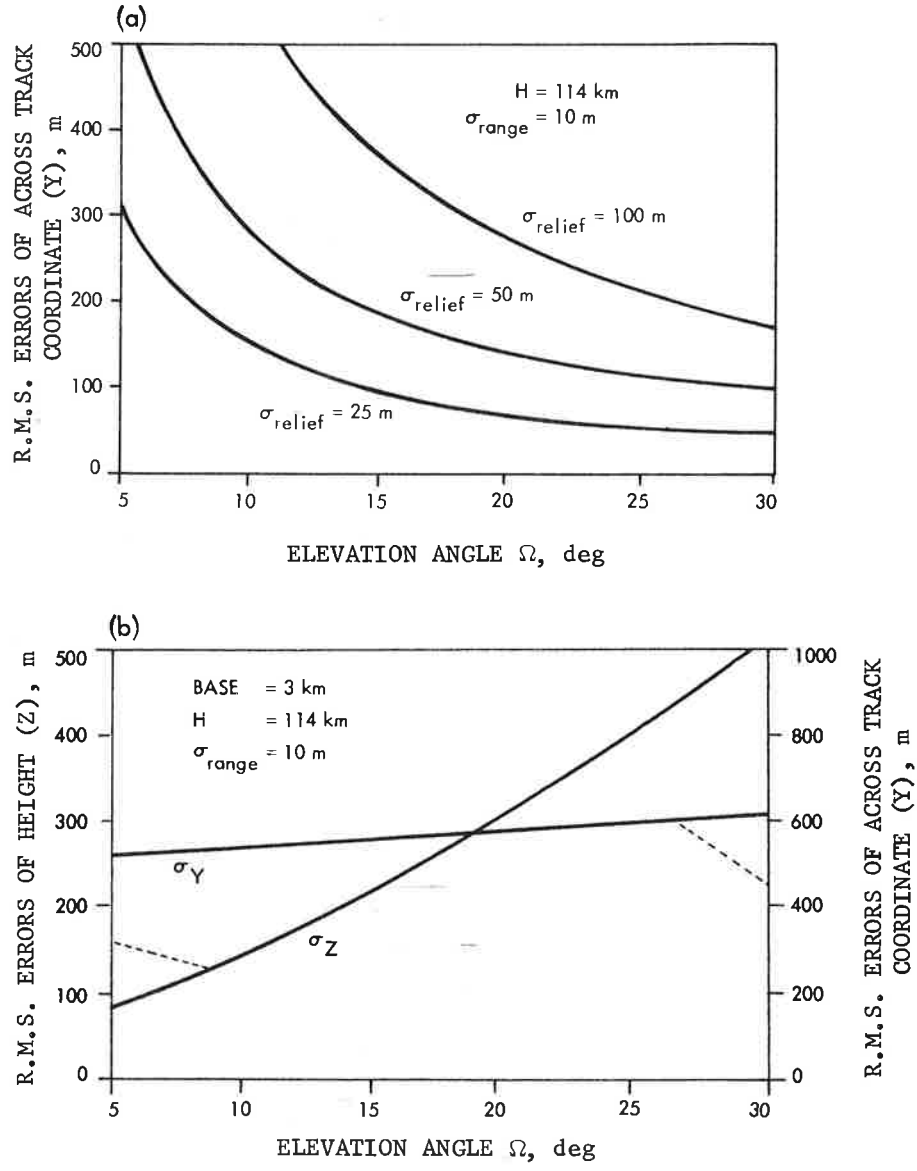

Fig. 6. Accuracy prediction of (a) single image and (b) stereo-radargrammetry.

source is the orbital altitude above a feature. These errors, of course, increase with smaller elevation angles of the line of sight. ALSE images were generated at rather small elevation angles; consequently, large mapping errors must be anticipated in the single-image approach due to variation of surface relief.

Radargrammetric stereo mapping (Figure 6b) produces rather accurate heights even with the small ALSE stereobase of 3 km and 2 deg angles of intersection of projection rays. However, this error increases rapidly with increasing elevation

angles. The cross-track coordinate Y, however, is rather erroneous (± 600 whatever the elevation angles. These errors can only be reduced with a la stereobase.

C. ACHIEVED RADARGRAMMETRIC ACCURACY

Table II presents the radargrammetric accuracy actually achieved with ALSE-V imagery, for single image and stereo mapping, respectively. The data are prese in a rectangular right-hand coordinate system with the Z-axis along the l normal at 19°N, 35.5°E, and the X-axis in orbit direction. If no ground con points are used (rows i), then the images can only very inaccurately be relate the orbit and the resulting mapping accuracy is rather low. Particularly planimetry, errors are up to ± 10 km in cross-track direction. If time marks of g quality would be available in the images, then these errors could be held m smaller. Accuracy can also significantly improve if only one ground control p is used. The single ground control point will eliminate most of the system error of the observed orbit and correct the relation between time marks orbit data. As a result, one obtains significantly reduced planimetric mapping er for both the single image and stereo approach (rows ii of Table II). He accuracy, however, does not drastically improve.

TABLE II

Root-mean-square differences between photogrammetric and radargrammetric coordinates of lunar features

		Single image			Stereo images			
Row	No. of control points	X, m	Y, m	No. of check points	X, m	Y, m	Z, m	No. of check points
i	0	9700	2010	49	9515	2570	344	65
ii	1	451	415	49	316	1260	332	65
iii	2	276	409	49	234	733	205	65
iv	8	160	362	49	173	510	109	65

Increasing the number of ground control points obviously increases also mapping accuracy. This holds to the extent to which control points describe nonlin orbit as well as image errors and, in the case of single-image mapping, the surf relief. Results achieved with ground control are not of great significance planetary exploration, where such control points are generally not availa However, the results obtained with a net of ground control points are representat of relative accuracy, since ground control essentially eliminates the absolut constant and linearly variable errors.

The effect of surface relief on single-image mapping is demonstrated by following numerical results. A root mean square variation of relief of ± 235 leads to an across track mapping error of more than ± 2 km. This error drops ± 233 m if the mapping area is flat to within a rms value of ± 56

Tiernan *et al.* (1976) also obtain an across-track mapping error of ± 250 m using a single ALSE-VHF image of Mare Serenitatis with a relief of ± 27 m. This conforms rather well to the theoretical accuracy prediction.

D. COMPARISON OF MAPPING METHODS

Tables IIIA and IIIB present a comparison of the different algorithms used for single-image and stereo radargrammetry. The single-image approach with little or no ground data should make use of the observed or predicted orbit and a calibration of range and time measurements. If, however, a large number of ground data are available, then it can be noted that interpolative use of ground control is about equivalent to parametric calibration.

TABLE IIIA

Comparison of radargrammetric mapping methods from single images

No. of ground control points	Simple formulation Eq. (18)		Predicted orbit interpolative use of ground points		Predicted orbit calibration of range and time	
	X, m	Y, m	X, m	Y, m	X, m	Y, m
0			9700	2010	9700	2010
1					451	415
2	320	670	330	579	276	409
8	152	360	132	358	160	362

Values are root mean square differences between photogrammetric and radargrammetric coordinates of lunar features.

TABLE IIIB

Comparison of radargrammetric mapping methods from stereo models

No. of ground control points	Simple formulation, Eq. (19)			Intersection of projection circles, Eq. (14)			Intersection of projection circles, Eq. (17)		
	X, m	Y, m	Z, m	X, m	Y, m	Z, m	X, m	Y, m	Z, m
0				9500	2570	344	9350	4610	800
1				316	1260	322	489	2457	639
2	581	660	550	234	733	205	255	2144	744
8	130	506	121	173	510	109	227	2095	630

Values are root mean square differences between photogrammetric and radargrammetric coordinates of lunar features.

Formation of a stereo model is most accurate with Equations (14), minimizing the square sum of the errors of the original observations. Equation (17), which minimizes the distance between two radar projection circles, cannot be used for stereo intersection. In many cases, the intersected radar model point has a large error, particularly in across track (Y) direction.

Radargrammetric intersection of stereo models using Equations (14) or (17) least squares problem, and weights have to be assigned to the observations. It found experimentally for Equations (14) that the observed range and sensor posi should be given about the same weight for optimum results. Equation produces the best result if the along-track component is given a smaller we than the across-track and height component. However, whatever the we assumption for Equations (17), the stereo model will be only very weakly defin

E. CONTOUR MAPPING

The coordinate most accurately determined by ALSE stereo radargrammetr height and not the planimetric coordinates X or Y. This is the result of steep look angle of the ALSE radar. Height accuracy reduces for shallower l angles (larger elevation angles). The good height accuracy of ALSE-radar ma it possible to attempt contouring of fairly small surface features. An example contours of Mons Maraldi is shown in Figure 7b together with phe grammetric contours (Figure 7a). These figures were obtained from an irreg digital height model. A regular grid of height points was interpolated and a stand computer contouring procedure applied.

Figure 7b displays only half of Mons Maraldi. The 2-m VHF radar did produce returns from the part of Mons Maraldi which slopes away from the anter Most of the electromagnetic energy was specularly reflected so that returns only received from the part of the surface sloping toward the orbit. A sho wavelength would have produced stronger diffuse returns from the backslopes would perhaps have permitted to generate a contourplot for the entire M Maraldi. The contour interval of 100 m used for Figure 7 is appropriate only the metric stereo model, but is too small for the radar stereo model. Si relative height accuracy was found to be ± 100 m, good cartographic practice wo suggest a minimum contour interval of 250 m or more to be appropriate for AL radar mapping.

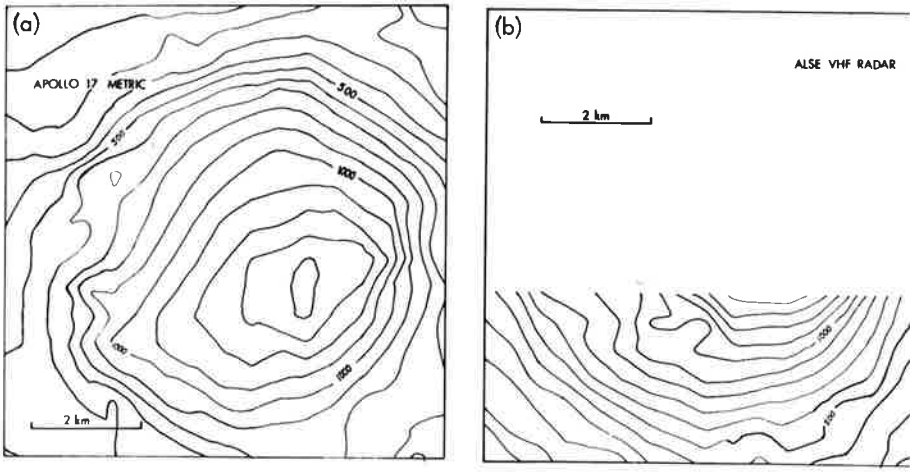

Fig. 7. Contour plots of Mons Maraldi procured from (a) Apollo 17 metric photography (b) ALSE-VHF radar.

4. Conclusions

A stereo-radargrammetric evaluation was carried out with the first, and thus far the only, set of civilian orbital radar images produced as part of the Apollo Lunar Sounder Experiment during the Apollo 17 mission to the Moon. Mapping of the lunar surface with these side-looking orbital radar images would be possible with a relative accuracy of ± 100 m in height and ± 250 to ± 500 m in planimetry. Absolute accuracy is about ± 300 m in height and ± 1 km to ± 2 km in planimetry. This height accuracy is superior to that obtained from planetary vidicon camera images, for example from Mariner 9, (Blasius, 1973). These results were obtained from a set of two overlapping VHF 2-m wavelength radar images of the area around crater and Mons Maraldi.

The rather good height accuracy, even with the small stereo base of 3 km available with the lunar radar images, is the result of the very steep look angles. Steep look angles will most probably be a characteristic of future orbital radar systems and will set them clearly apart from airborne radar with near grazing look angles (Derenyi, 1975).

Not only stereo-radargrammetric but also single-image radar mapping was evaluated. The single-image approach is sensitive to deviations of the relief from its assumed reference. A rather flat surface can be mapped from a single orbital ALSE radar image with an accuracy of ± 250 m. This value was also obtained by Tiernan *et al.* (1976). But for even only moderate relief (rms relief of ± 250 m), the mapping accuracy reduces to more than ± 2 km.

The relative accuracy of radar mapping from both single and stereo images is limited basically by the radar geometry. The absolute accuracy, however, is determined by the error of the observed spacecraft trajectory. A study of various alternative radar stereo configurations should reveal how much can be gained in relative mapping accuracy beyond that demonstrated with the Apollo 17 ALSE images. Such an analysis would be valuable, particularly for planning a Venus Orbiting Imaging Radar (VOIR) mission.

Acknowledgment

I am grateful to Mr Sherman Wu and his colleagues at the Center for Astrogeology of the U.S. Geological Survey, Flagstaff, Arizona, for making available their equipment, time and expertise for the radargrammetric and photogrammetric measurements. For help in solving many problems with the ALSE data and Apollo 17 orbit parameters, I am indebted to M. Tiernan, L. Roth, and Dr W. Sjogren of JPL.

References

Baker, J. R., Marks, G. W., and Mikhail, E. M. 1975, 'Analysis of Digital Multispectral Scanner (MSS) Data', *Bildmessung und Luftbildwesen*, Vol. 43, No. 1, Karlsruhe, W. Germany.

Blasius, K.: 1973, 'A Study of Martian Topography by Analytic Photogrammetry', *J. Geophys. Res.* **78**.

Derenyi, E. E.: 1975, 'Terrain Heights from SLAR Imagery', presented at the 41st Annual Meeting of the American Society of Photogrammetry, Washington, D.C., March 9–14.

Gracie, G., Brewer, R., *et al.*: 1970, *Stereo Radar Analysis*, Final Technical Report, Contract DACA 76-69-C-0002, ARPA Order No. 1229, Raytheon Autometric Operation.

Konecny, G.: 1970, 'Metric Problems in Remote Sensing', in *Proceedings of the ISP-Comm Symposium*, Delft, ITC-Publication, Series A, No. 50, Delft, Netherlands.

Leberl, F.: 1970, 'Evaluation of Single Strips of Side-Looking Radar Imagery', invited paper, C mission IV, 12th Congress of the International Society of Photogrammetry, Ottawa, Canada.

Leberl, F.: 1975, 'Lunar Radargrammetry with ALSE-VHF Imagery', *Proceedings of the Fall Tech Meeting*, American Society of Photogrammetry, Phoenix, Arizona, October 26–31.

Phillips, R., Adams, G. F., *et al.*: 1973, 'Apollo Lunar Sounder Experiment', *Apollo 17 Prelimi Science Report*, NASA SP-330, Washington, D.C.

Rose, J. R. and Friedman, L. D.: 1974, 'A Design for a Venus Orbital Imaging Radar Miss American Institute of Aeronautics and Astronautics, AIAA Paper No. 74-222, 12th Aeros Sciences Meeting, Washington, D.C., January 1974.

Tiernan, M., Roth, L., Thompson, T. W., Elachi, C., and Brown, W. E., Jr.: 1976, 'Lu Cartography with the Apollo 17 ALSE Radar Imagery', *The Moon* **15**, 155.